Einstein Telescope
and a future on the Moon

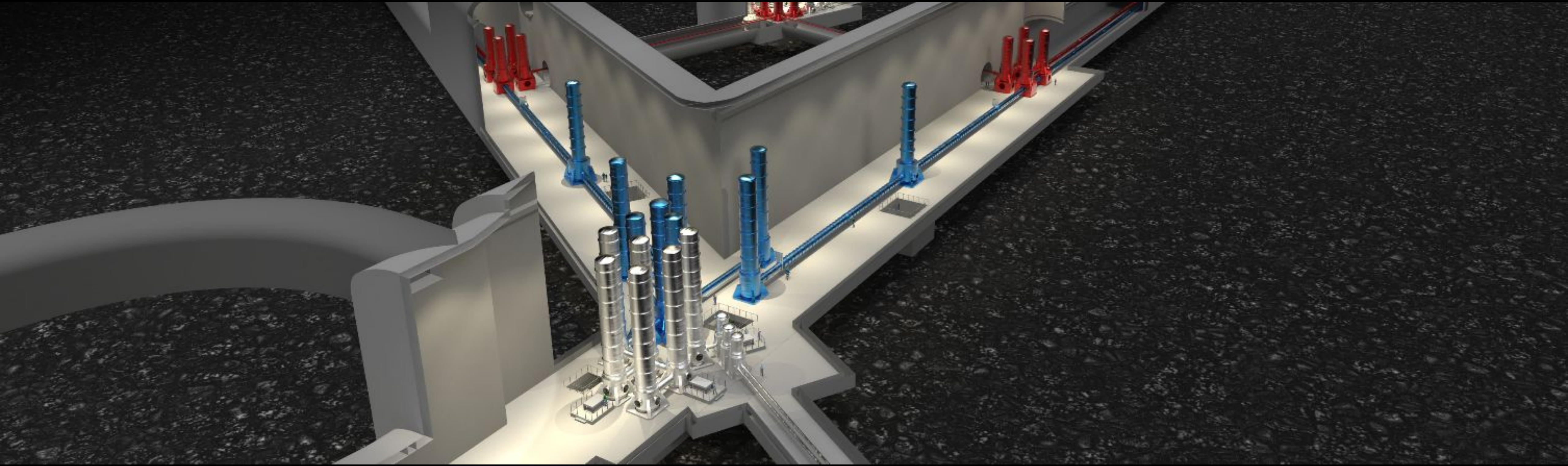

Jan Harms

Gran Sasso Science Institute

Einstein Telescope

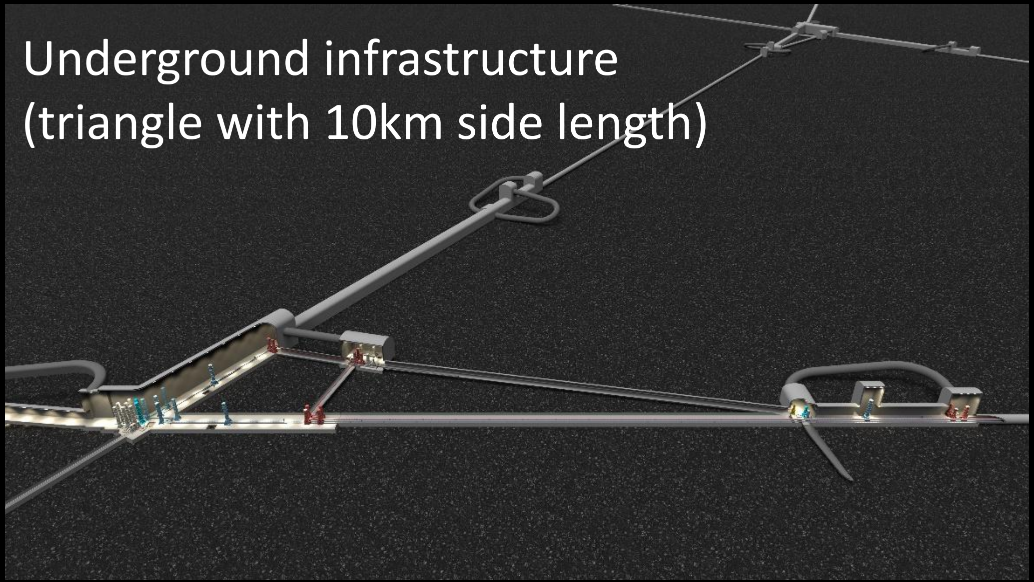

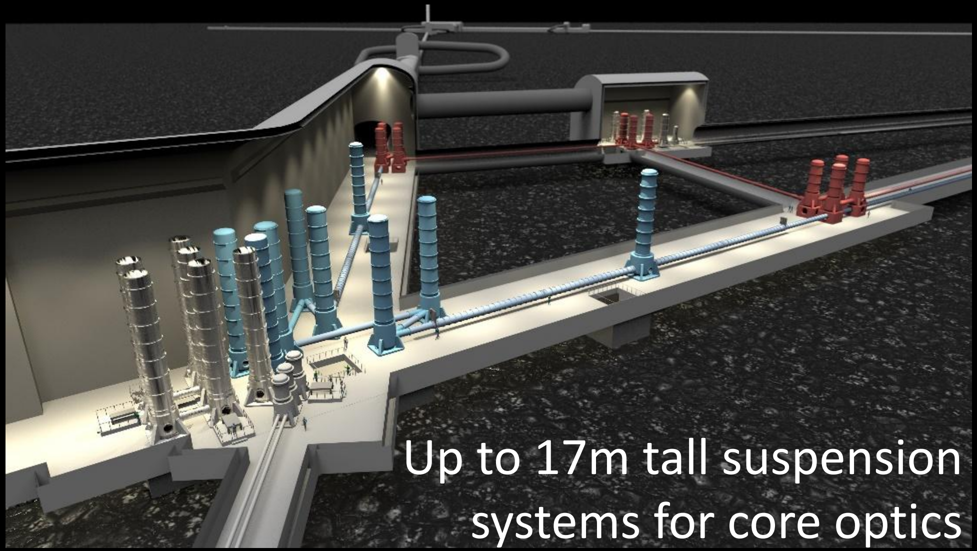

Site Studies

Active seismic survey

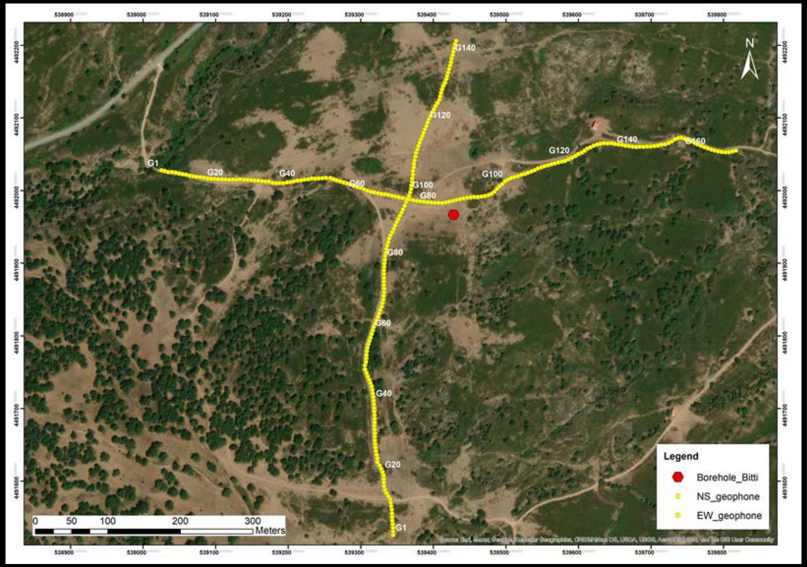

Geotechnical
Geological
Hydrological
Geophysical

Lowering of borehole seismometer

Drilling of borehole

Example result from an active seismic survey

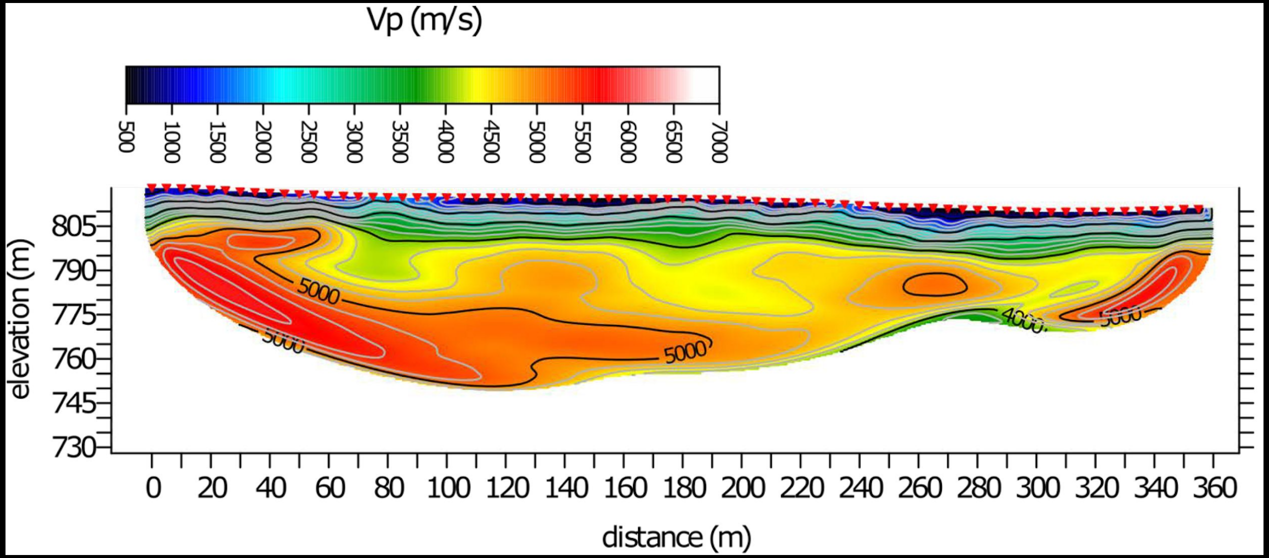

ETpathfinder

New facility in Maastricht to learn operating a laser interferometer at cold temperatures.

Einstein Telescope as Xylophone

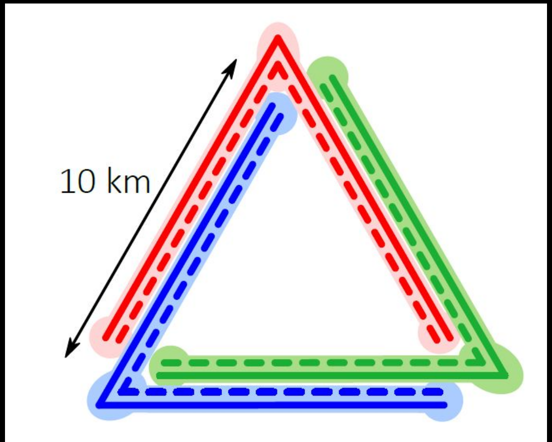

Each vertex is the center of a pair of interferometers, i.e., 6 interferometers in total.

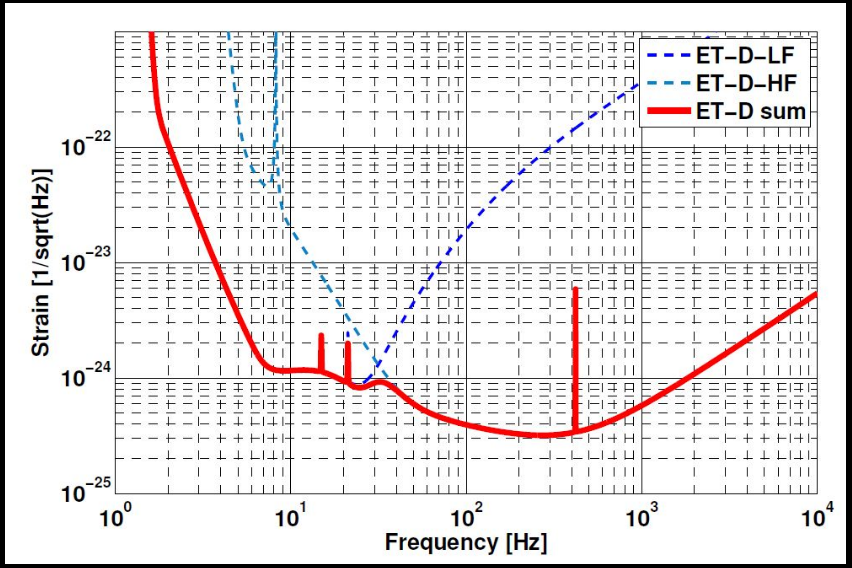

Power: 18kW
Temperature: 10-20K

Power: 3MW
Temperature: 290K

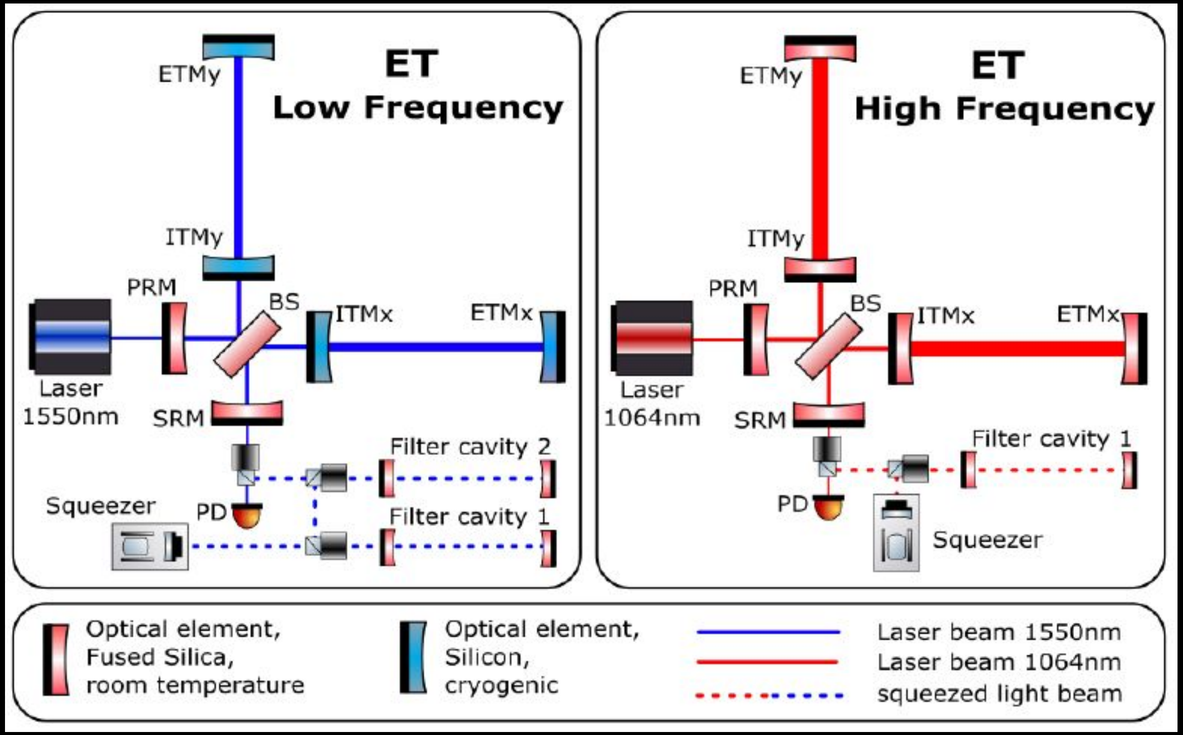

Main ET Design Parameters

Parameter	ET-HF	ET-LF
Arm length	10 km	10 km
Input power (after IMC)	500 W	3 W
Arm power	3 MW	18 kW
Temperature	290 K	10-20 K
Mirror material	fused silica	silicon
Mirror diameter / thickness	62 cm / 30 cm	45 cm/ 57 cm
Mirror masses	200 kg	211 kg
Laser wavelength	1064 nm	1550 nm
SR-phase (rad)	tuned (0.0)	detuned (0.6)
SR transmittance	10 %	20 %
Quantum noise suppression	freq. dep. squeez.	freq. dep. squeez.
Filter cavities	1×300 m	2×1.0 km
Squeezing level	10 dB (effective)	10 dB (effective)
Beam shape	TEM_{00}	TEM_{00}
Beam radius	12.0 cm	9 cm
Scatter loss per surface	37 ppm	37 ppm
Seismic isolation	SA, 8 m tall	mod SA, 17 m tall
Seismic (for $f > 1$ Hz)	$5 \cdot 10^{-10}\ \mathrm{m}/f^2$	$5 \cdot 10^{-10}\ \mathrm{m}/f^2$
Gravity gradient subtraction	none	factor of a few

Geometry of an ET Vertex

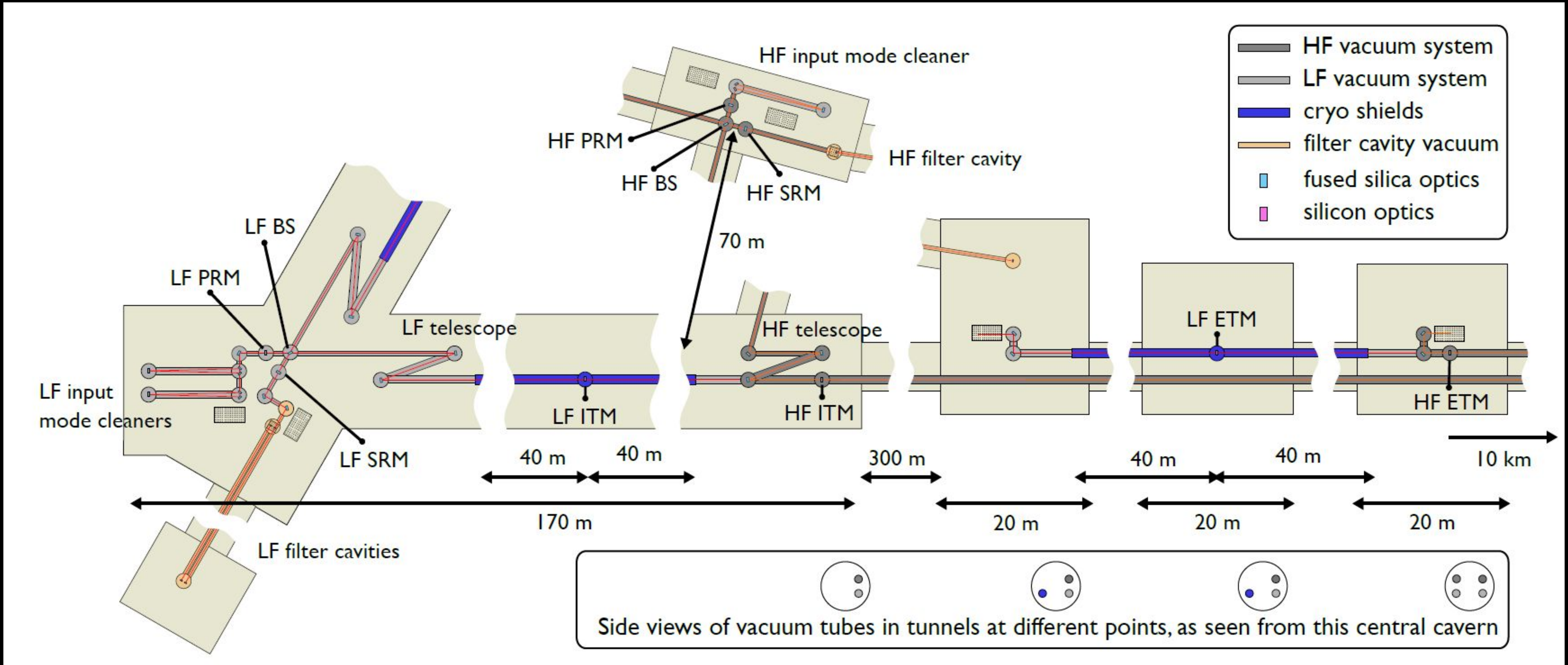

Underground Infrastructure Noise

Typical seismic spectrum at an underground research facility (ex LNGS)

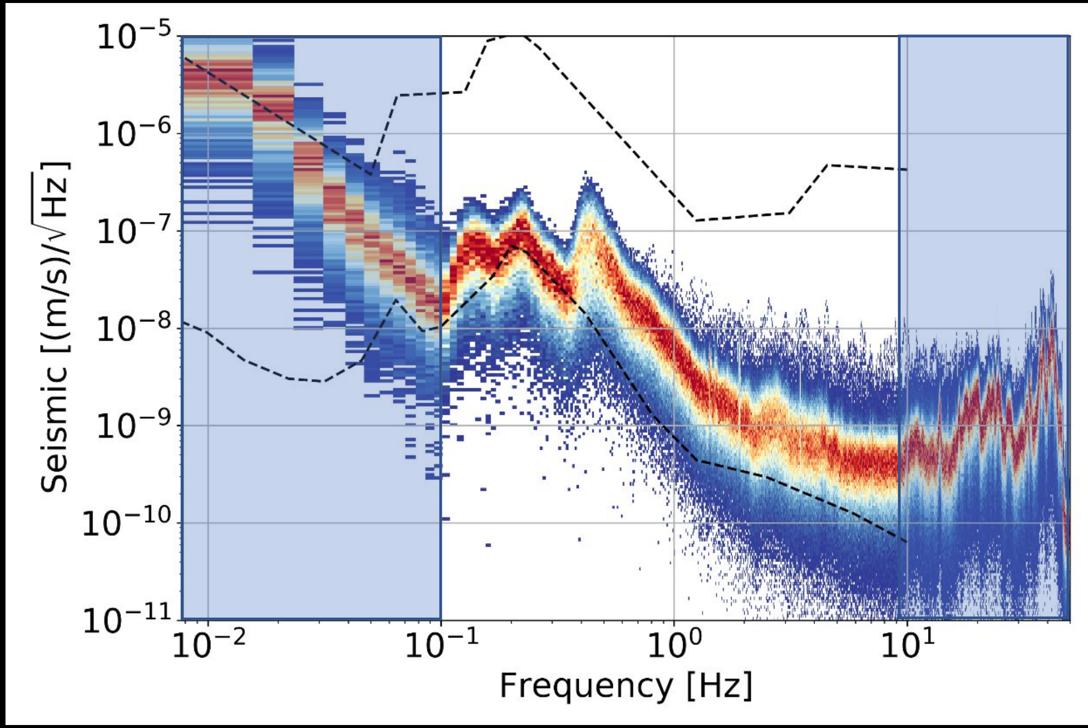

Machines

Somehow produced by pressure fluctuations. Potential connection to ventilation system.

Vacuum pumps

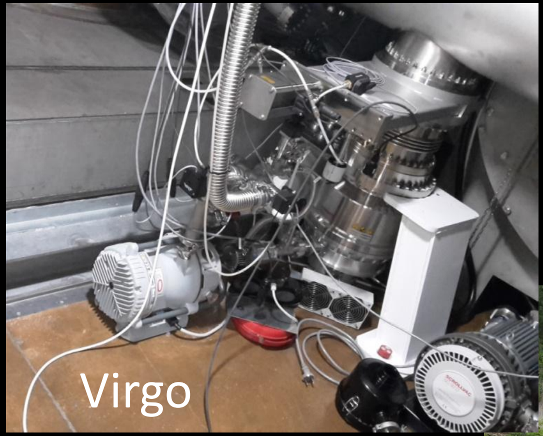

Ventilation

Cryocooler

Newtonian Noise

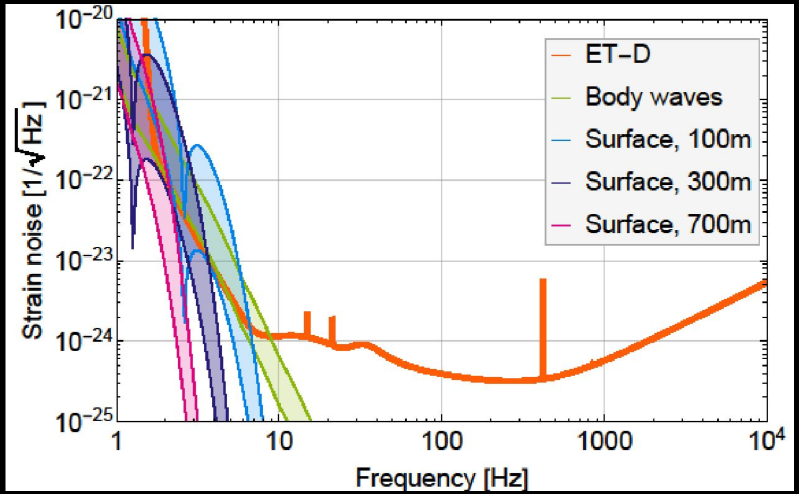

Underground construction greatly reduces, but does not completely remove, Newtonian noise.

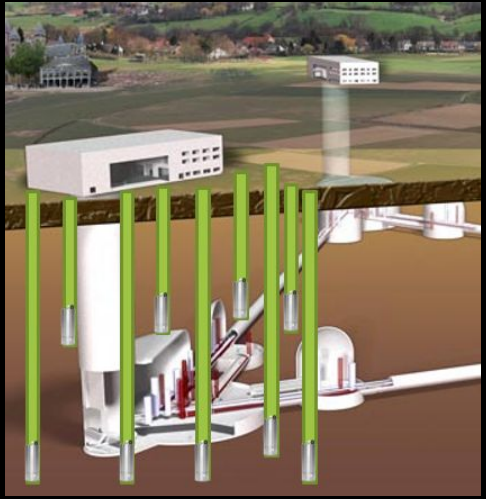

Newtonian noise must be subtracted using data from sensor networks. Most complicated subsystem of Einstein Telescope.

Finite-element simulations

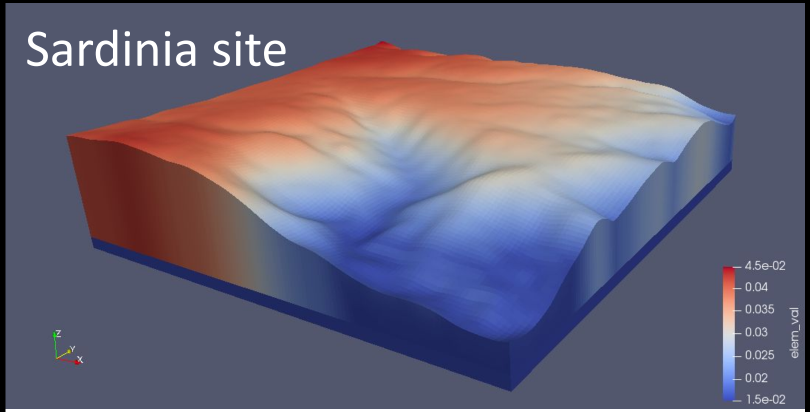

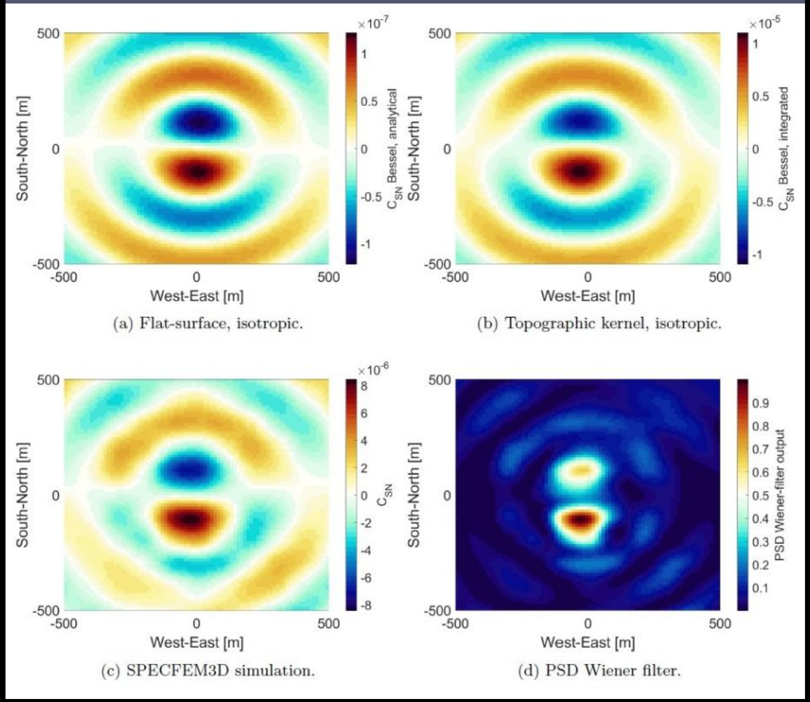

Sensitivity Goals of the Next-Generation Facilities

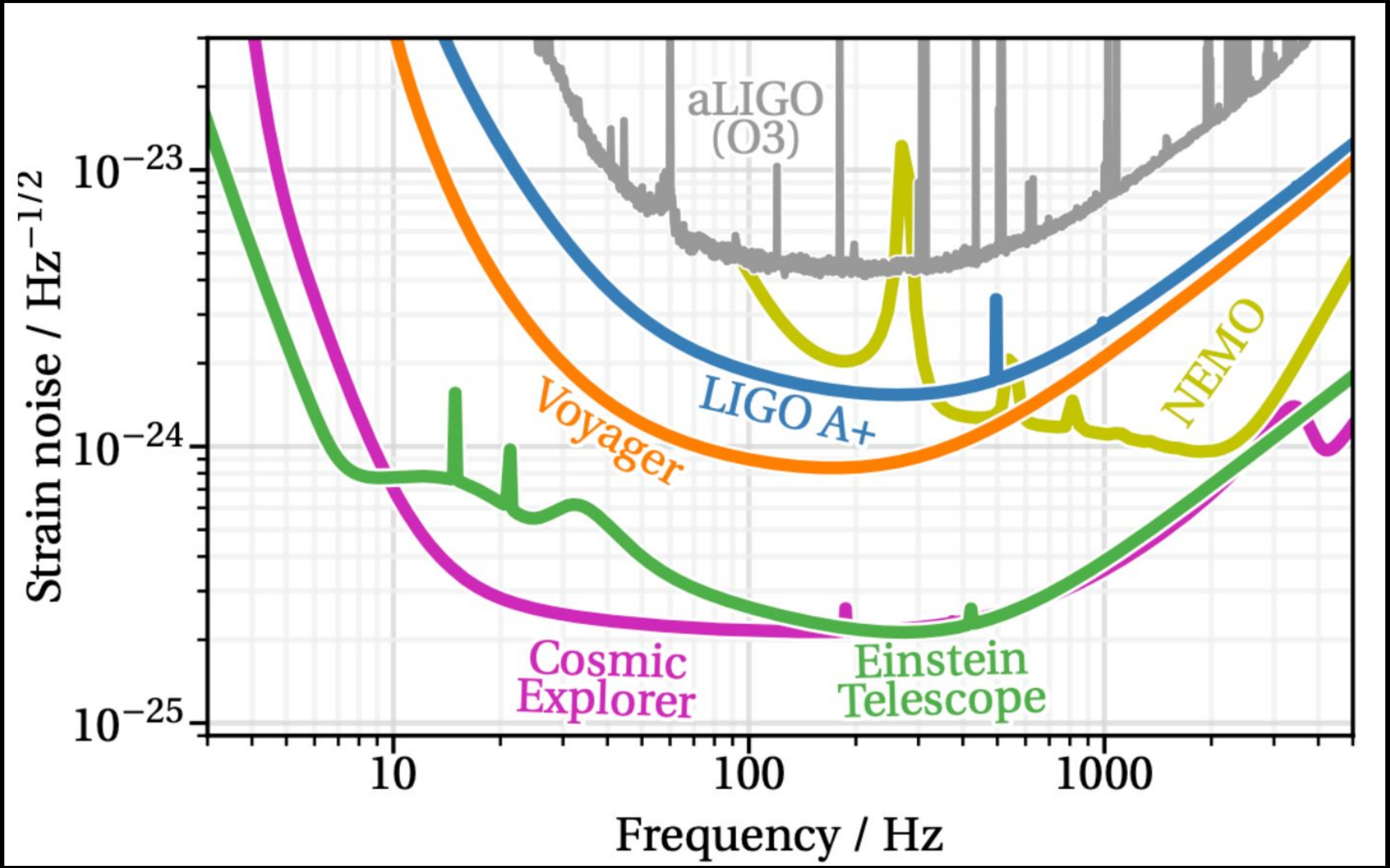

Binary BH Detection Horizon

Current infrastructure (Virgo, LIGO, KAGRA) z=2

Next-generation infrastructure (Einstein Telescope, Cosmic Explorer) z=100

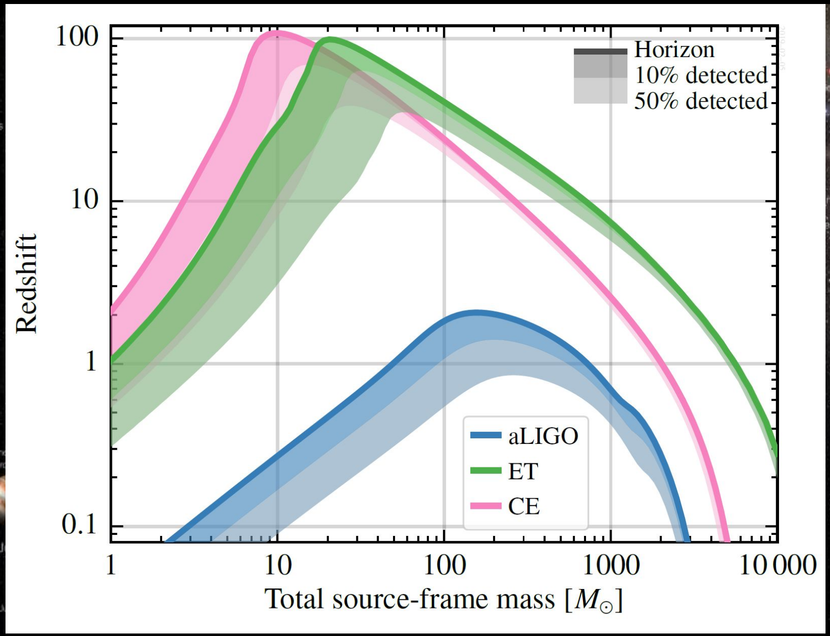

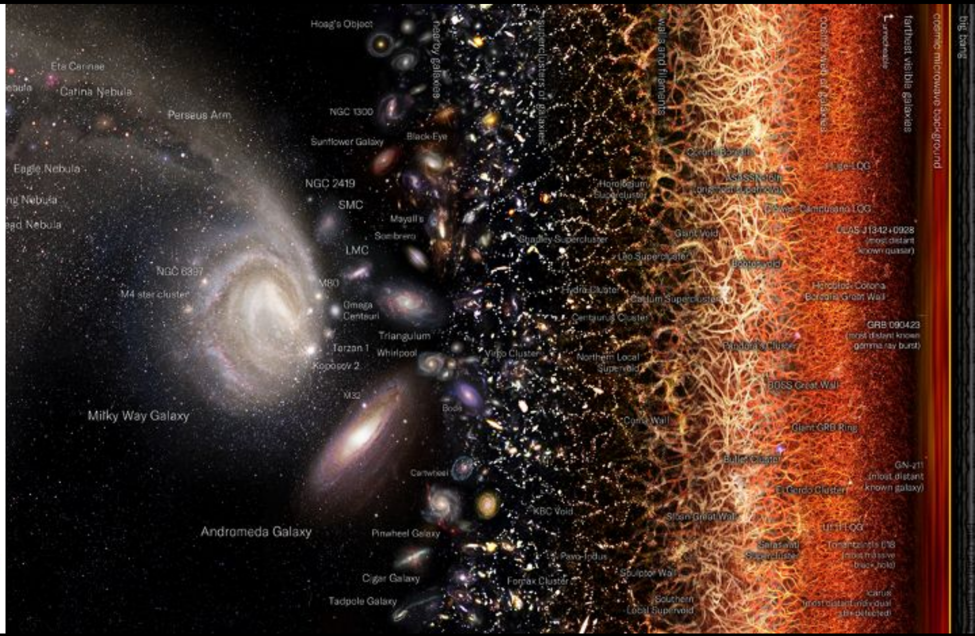

Logarithmic distance scale, Pablo Carlos Budassi

Sheer Numbers

O1: 12.9.2015 – 19.1.2016

O2: 30.11.2016 – 25.8.2017

O3a: 1.4.2019 – 30.9.2019

O3b: 1.11.2019 –26.3.2020

ET is expected see about
10^5 BNS and 10^5 BBH per year

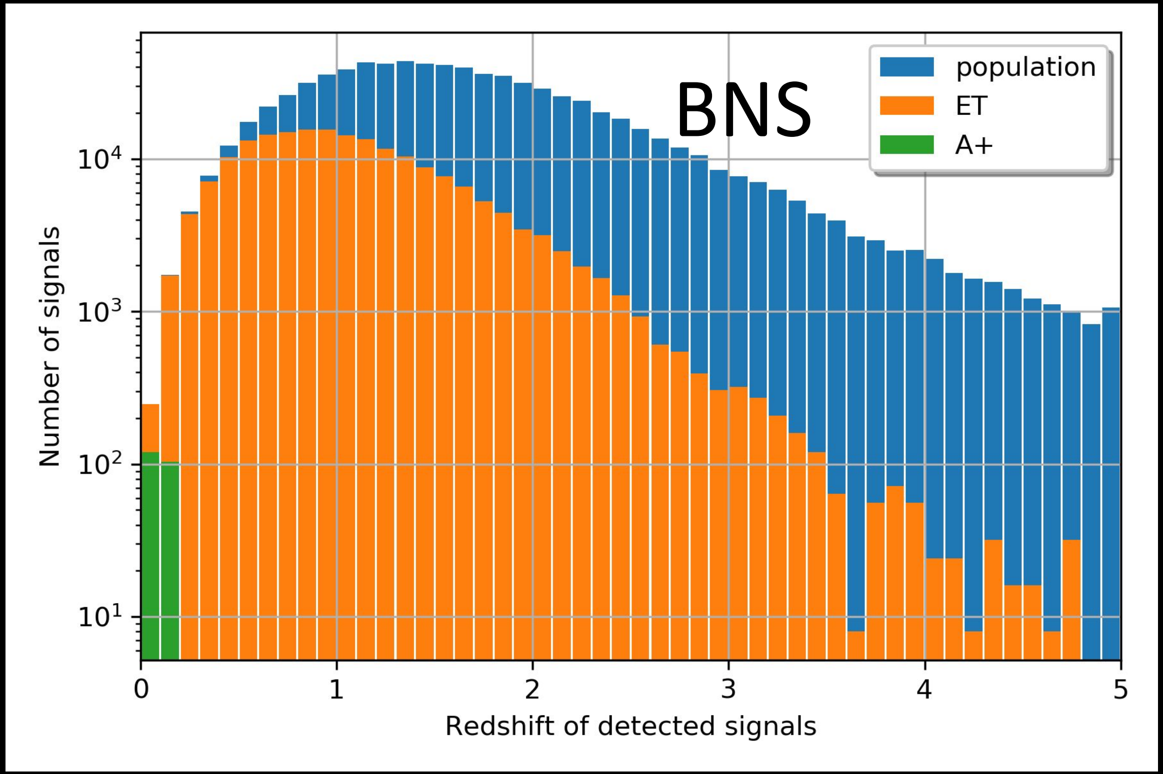

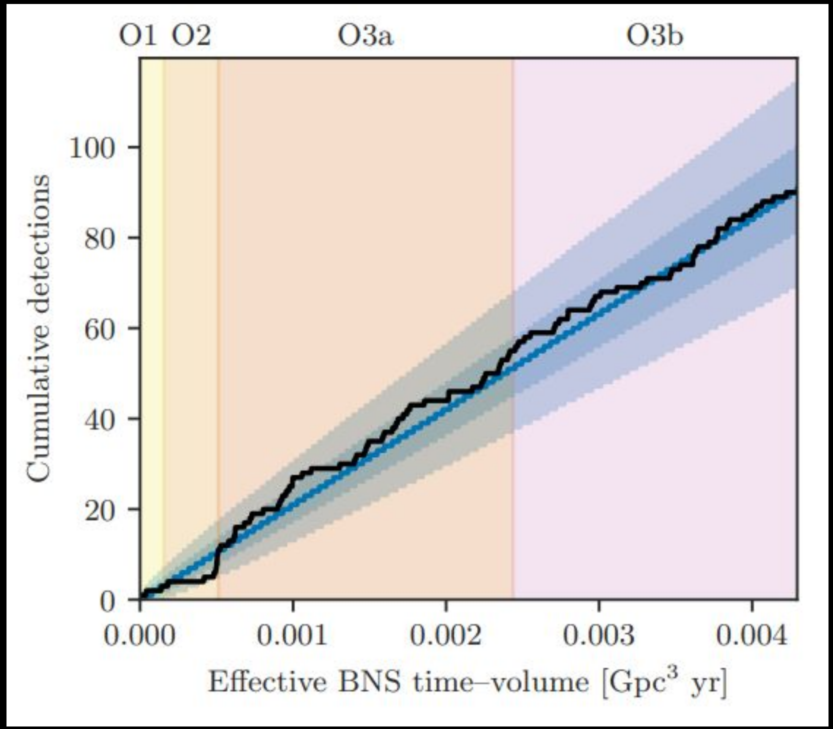

Science Of Neutron Stars

Radioactively powered transients

Nucleosynthesis

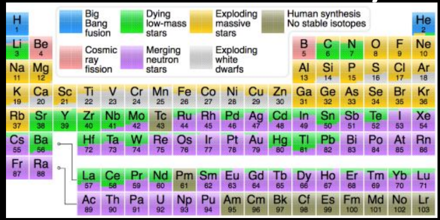

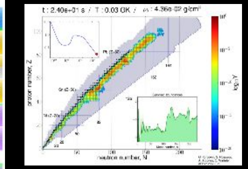

Relativistic astrophysics

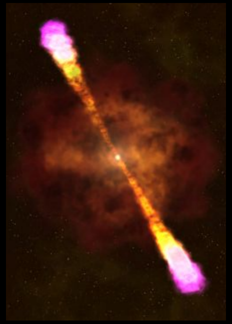

Credit: M Branchesi

Compact-object formation and evolution

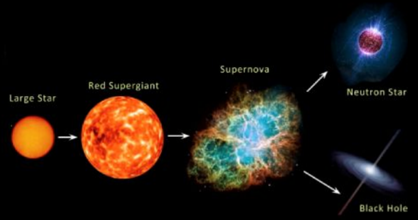

Cosmology

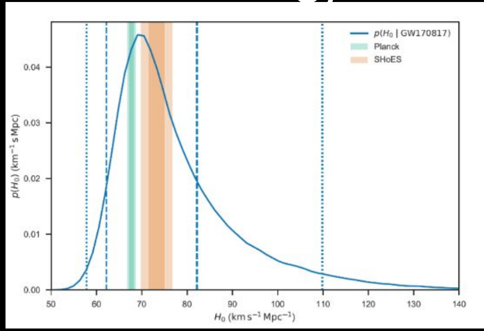

Nuclear matter physics

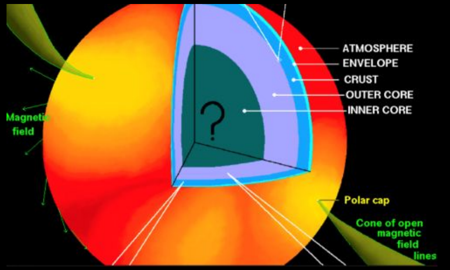

Black-hole populations

Observing of order 10^5 BBH mergers, population models can be analyzed precisely as a function of redshift.

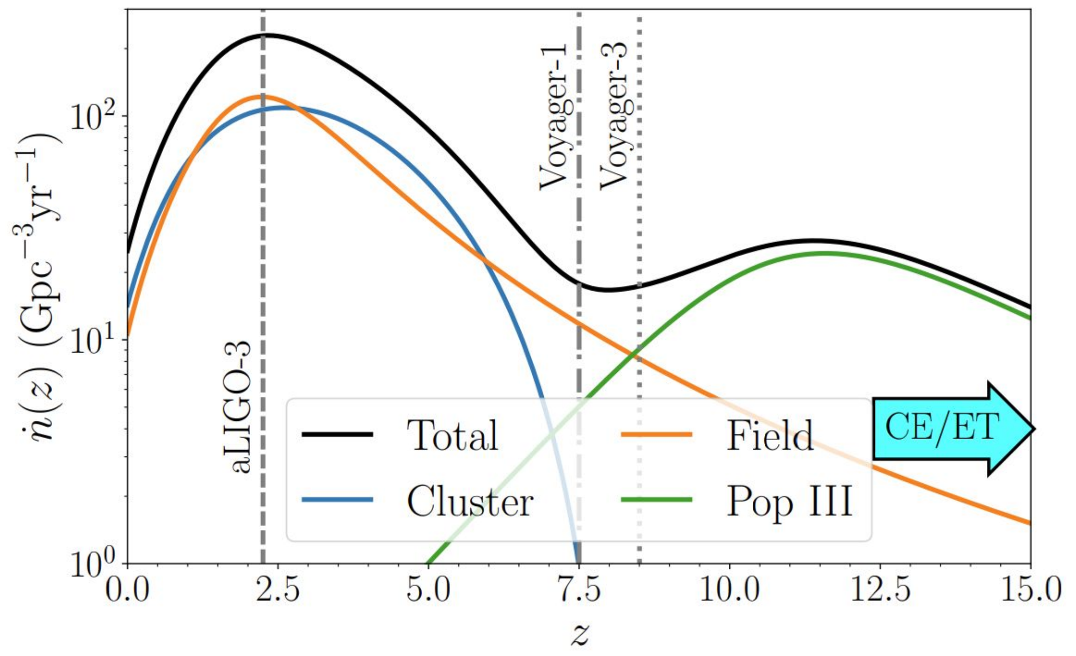

Ng et al, 2021

Existence of a primordial BH population is speculative. A challenge will be to tell Pop III from primordial BBHs.

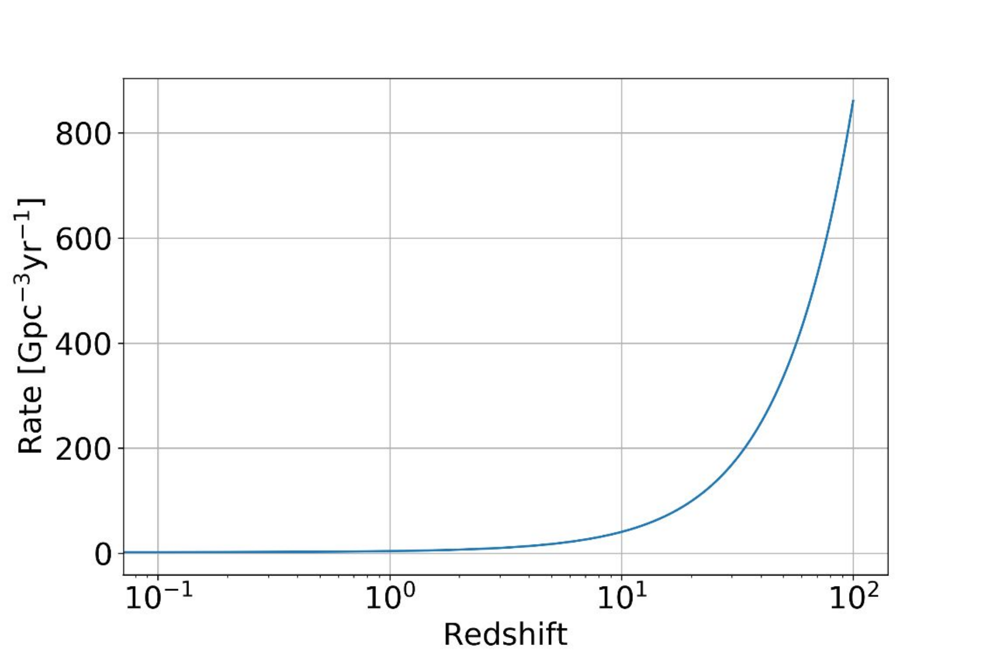

De Luca et al, 2020

Individual BBH Signals: New Physics

BH superradiance with light bosons

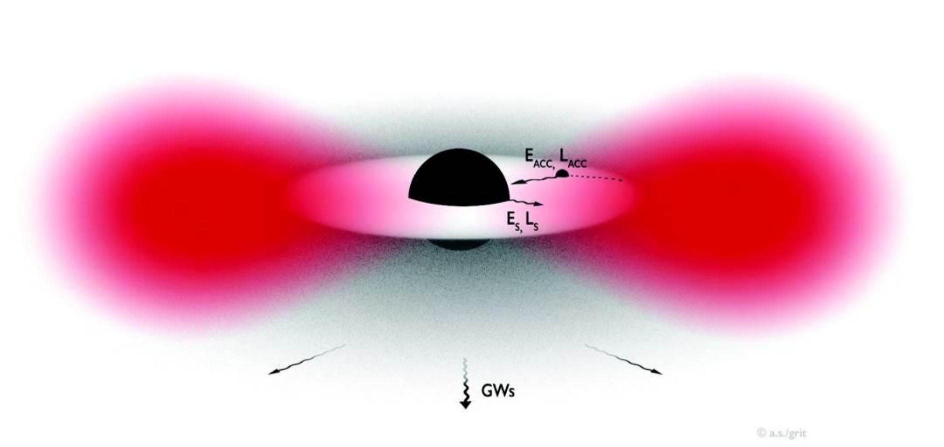

Black holes: the ultimate engine of discovery [cit Cardoso, 2020]

Probing the structure of BH spacetime

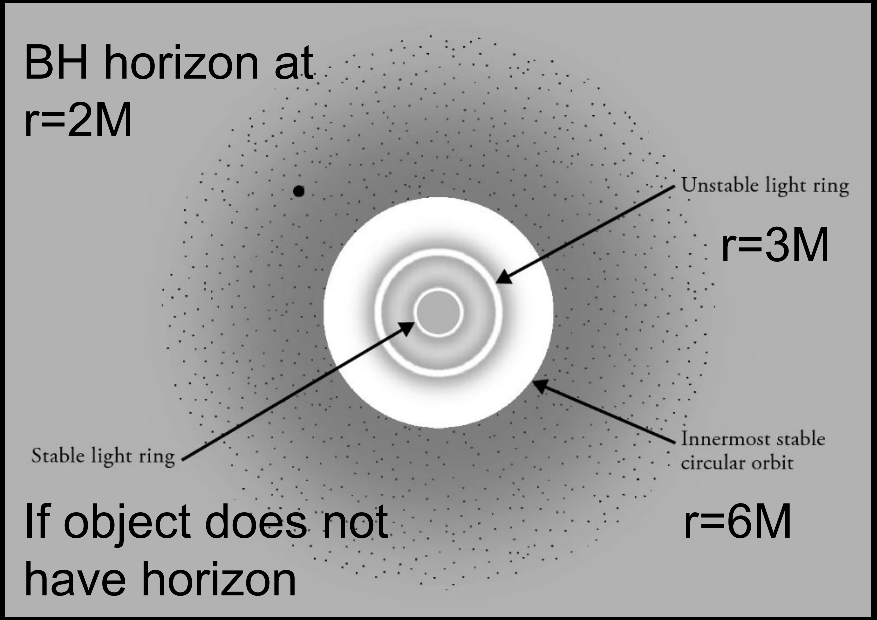

Cardoso, Pani, 2019

Exotic compact objects: Infer mass-radius relation

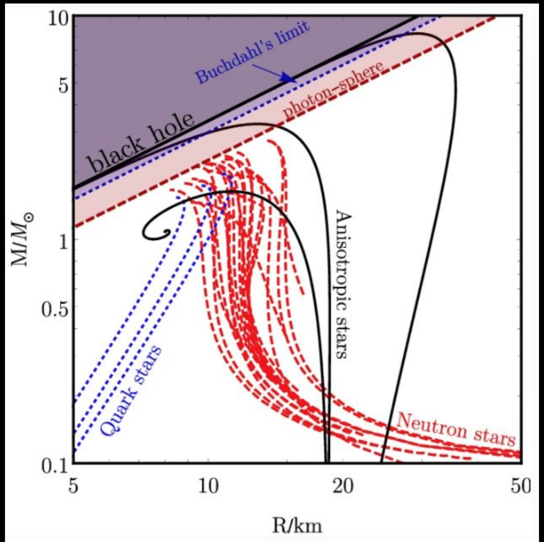

Cardoso, Pani, 2019

Quantum gravity: area discretization

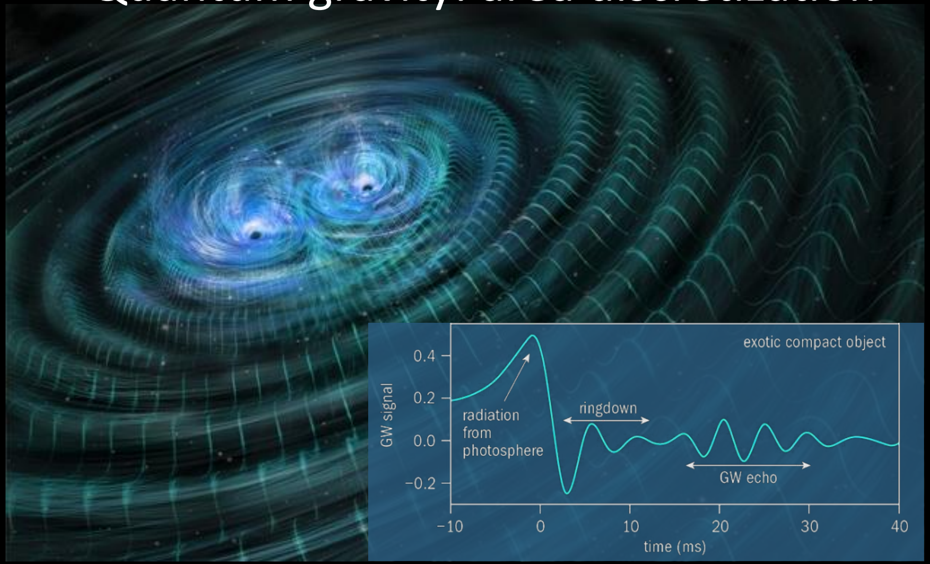

Agullo et al, 2021

Quadrupolar vibration induced by a GW
(here showing spheroidal mode)

Past Planetary GW Detectors

Data from N.32°W.
Benioff strain seismograph at Isabella, CA

No. 4763 February 11, 1961 NATURE

LETTERS TO THE EDITORS

GEOPHYSICS

Upper Limit for Interstellar Millicycle Gravitational Radiation

ROBERT L. FORWARD*
DAVID ZIPOY
J. WEBER
Department of Physics, University of Maryland, College Park, Maryland.
STEWART SMITH
HUGO BENIOFF
Seismological Laboratory, California Institute of Technology, Pasadena, California.

$$\overline{\varepsilon(t)^2} \approx \frac{4c^4Q}{\pi^2\omega^3} R^2_{iojo}(\omega) = \frac{60GQ}{c^3\omega} t_{or}(\omega) \quad (2)$$

In equation (2), $R^2_{iojo}(\omega)$ is the power spectrum of the Riemann tensor, G is the constant of gravitation

Upper limits on Riemann-tensor power spectrum

Table 1

Fundamental mode	Period (min.)	Q (est.)	Strain² (av.)	$R^2_{iojo}(\omega)$ $\left[\frac{1}{\text{cm.}^4\ (\text{rad./sec.})}\right]$	$t_{or}(\omega)$ $\left[\frac{\text{watts}}{\text{cm.}^2\ (\text{rad./sec.})}\right]$
S_2	54·0	400	80×10^{-25}	$< 0·5 \times 10^{-75}$	< 20
S_4	25·8	350	20	2	20
S_6	16·0	300	8	3	10
S_8	11·81	250	4	5	10
S_{10}	9·66	210	2·5	7	10
S_{14}	7·47	180	1·2	10	10
S_{20}	5·78	160	1	20	10
S_{30}	4·37	120	0·6	30	10
S_{38}	3·66	100	0·6	60	10

Multiply with $8 \cdot 10^{49} \cdot (1\text{mHz}/f)^4$ to get GW strain PSD

NASA, Apollo 17 (1972)

The **Lunar Surface Gravimeter** would have set the most stringent limits on the energy of a GW background at that time, but it had greatly reduced sensitivity due to a design flaw.

It was then determined that an error in arithmetic made by La Coste and Romberg, and known to the firm's highest officials, had not been corrected by La Coste and Romberg. This led to an instrument which had excellent performance in earth g and was just barely outside of the tolerances for variations of lunar site g. This error resulted in the

Lunar GW Detector Concepts

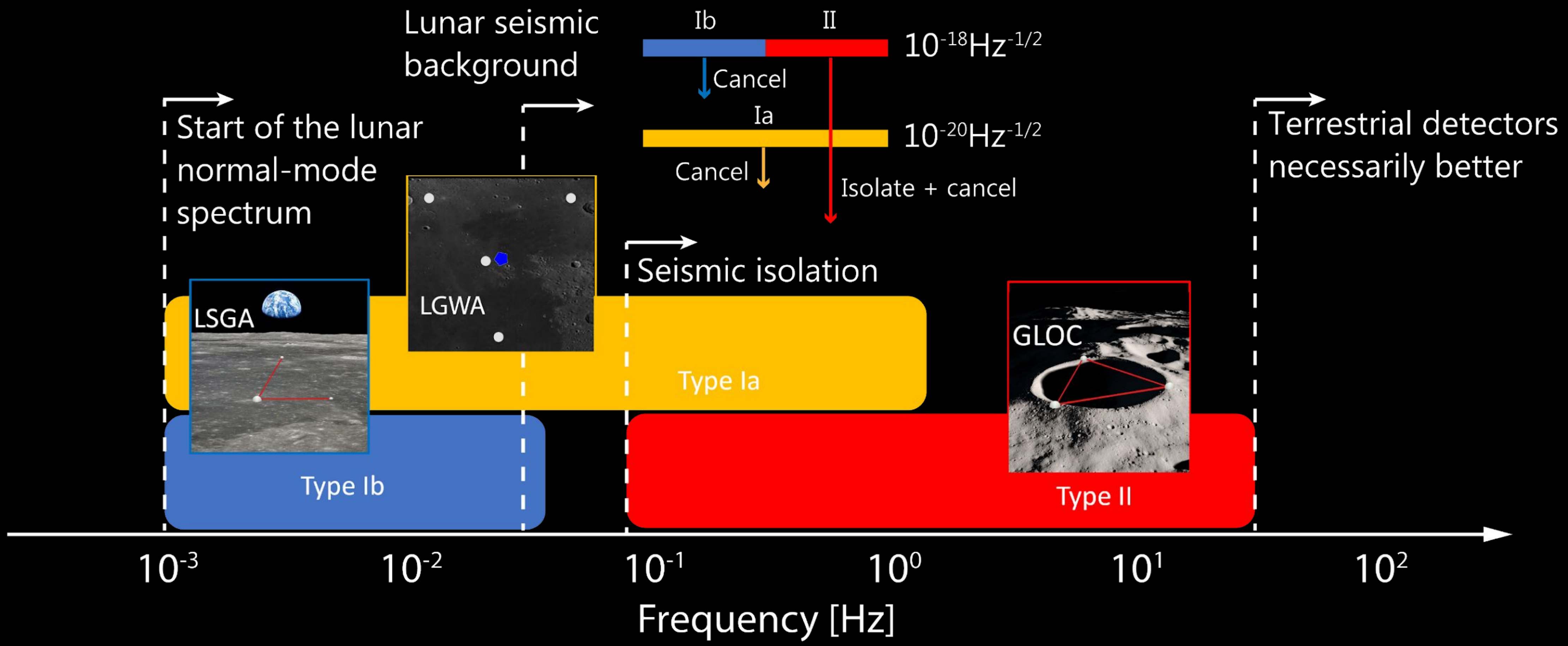

LGWA Concept

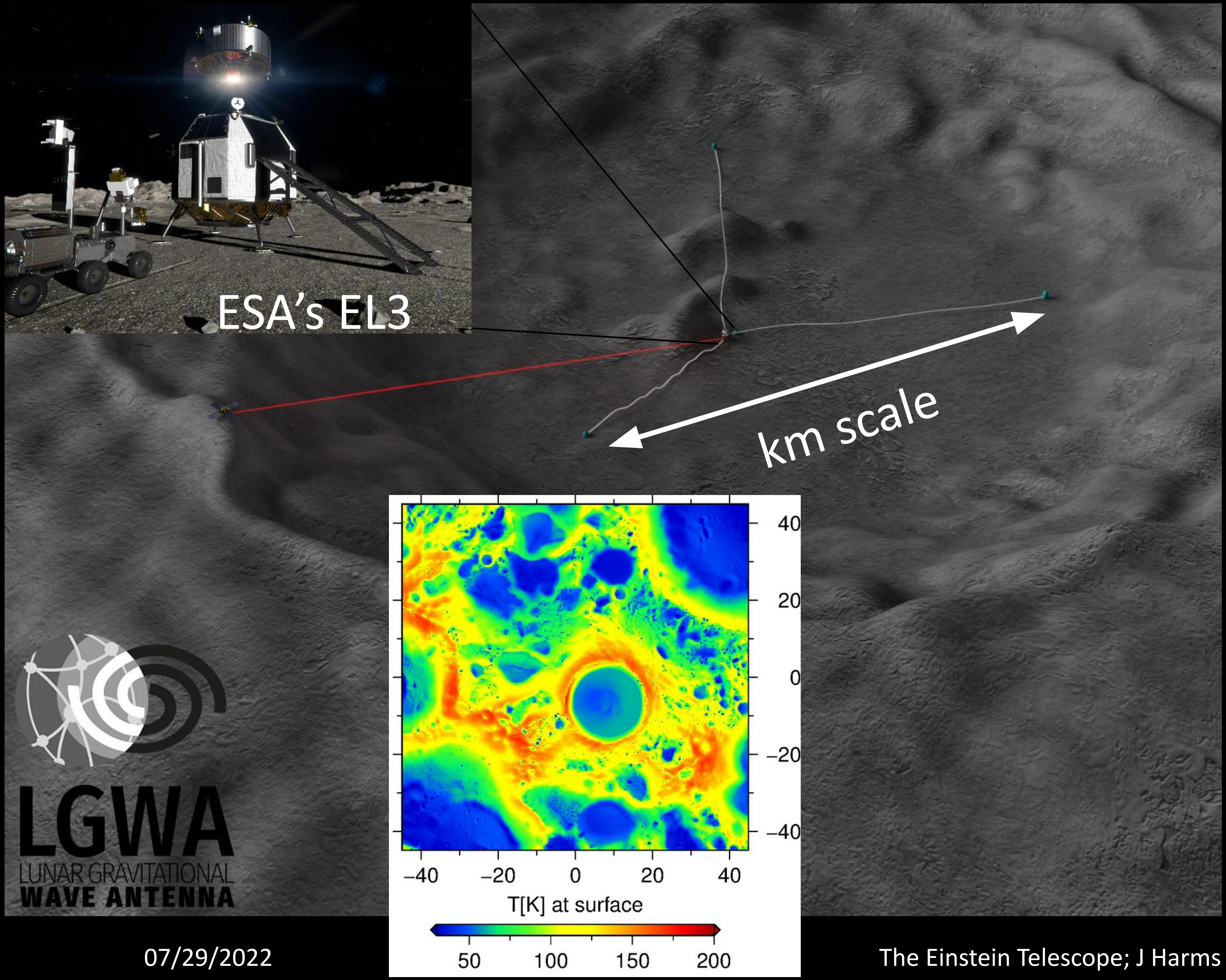

Lunar seismic spectra

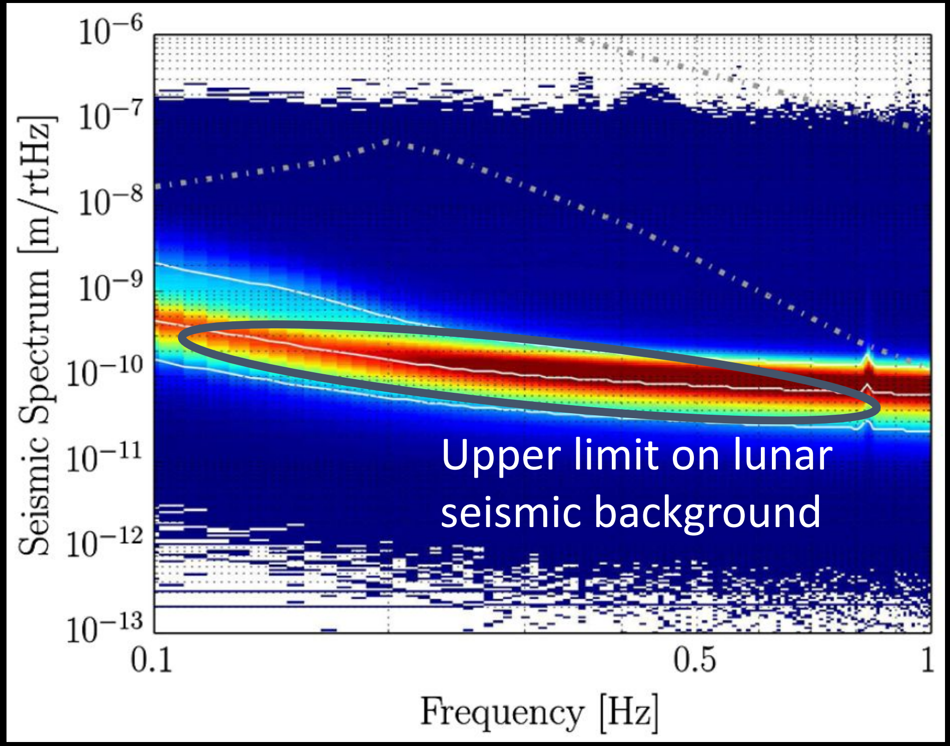

- Extremely weak seismic background
- Use coherent noise cancellation to further reduce seismic background noise in data

Multiband GW Observations

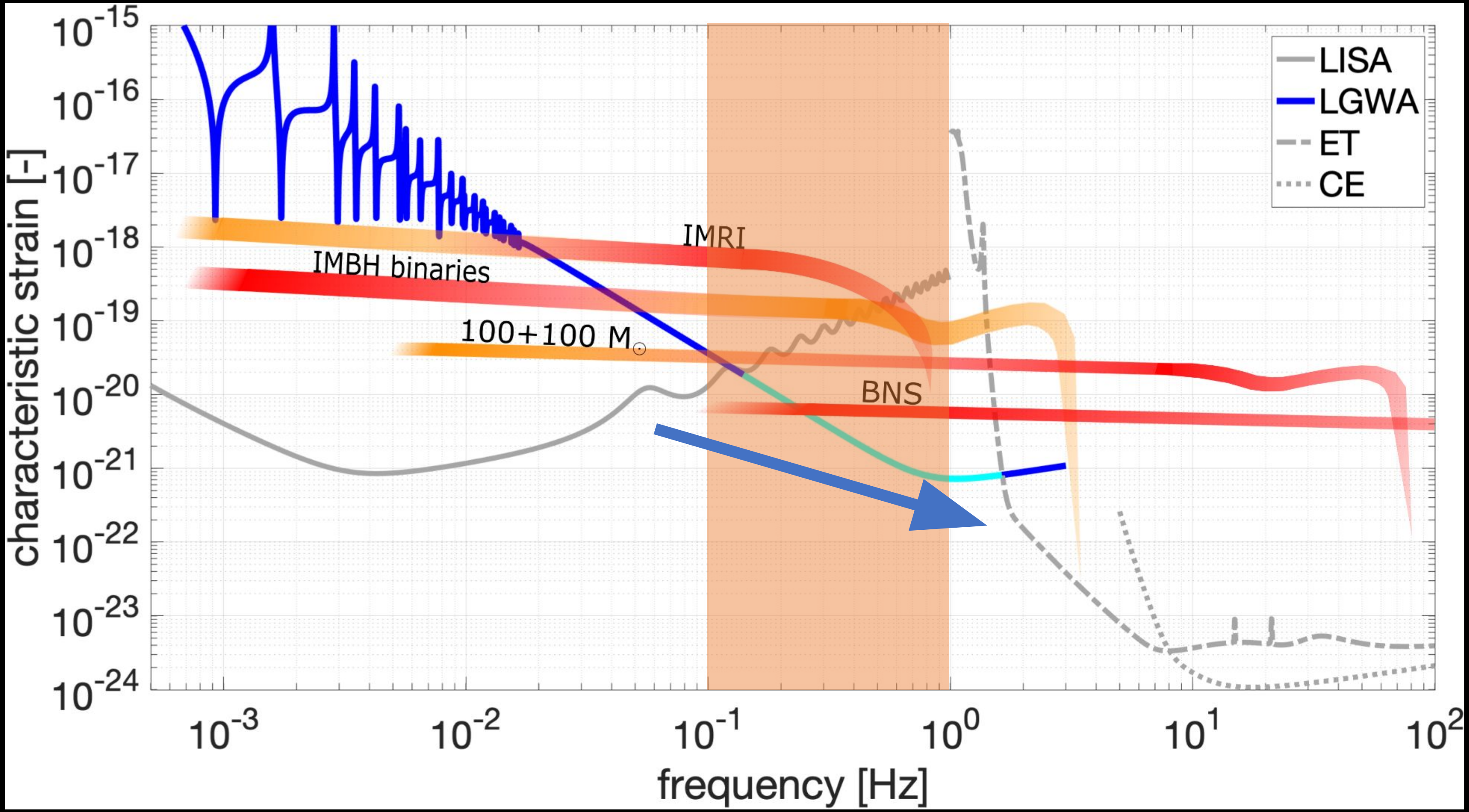

LGWA Science